

# Peer-Reviewed Technical Communication

## Wave Propagation Prediction Over a Thin Elastic Sediment and Rock Basement

Cathy Ann Clark, *Senior Member, IEEE*

**Abstract**—In this paper, a model which computes both compressional- and shear-wave transmissions and reflections through a sediment layer is utilized to formulate a single bottom reflection coefficient which is shown to successfully predict resonance effects due to shear-wave conversion in various types of sediment. Comparisons of model results to published bottom loss curves are presented. Propagation results obtained by implementing the bottom loss calculations in a normal mode model are compared to other model results and measured data sets over a variety of bottom types.

**Index Terms**—Acoustics, bottom sediment propagation, elastic media, shear, underwater sound propagation, wave equation.

### I. INTRODUCTION

THE effect of elastic sediment properties on underwater acoustic propagation has been an area of active research for decades. Two papers by Vidmar, published in 1980, analyzed the effects of sediment shear-wave propagation on acoustic bottom loss by numerical integration of the wave equation [1], and by a ray path decomposition method based on expansion of the reflection and transmission coefficients as a function of a parameter defined by the ratio of the sediment shear sound speed to the compressional sound speed in the water [2]. The dependence of loss on compressional-to-shear conversion and the resultant high losses at low and resonance frequencies were measured and studied by a number of researchers throughout the 1980s [3]–[12]. Reflection and refraction coefficients for a plane wave at a solid plane layer for the liquid–solid–liquid case were expanded into series representations by Deschamps and Cao in 1991 [13], and the case of a thin anisotropic layer between two anisotropic solids was published by Rokhlin and Huang in 1992 [14]. Also in 1992, Hovem and Kristensen showed that Stonely interface waves excited by evanescence from compressional-waves incident on the sediment at angles below critical can also account for these high losses, without shear-wave conversion [15].

Manuscript received December 01, 2010; revised July 25, 2011 and March 08, 2012; accepted March 26, 2012. Date of publication May 15, 2012; date of current version July 10, 2012. This work was supported by the U.S. Office of Naval Research under the FY10 In-house Laboratory Independent Research Program, administered by the Naval Undersea Warfare Center (NUWC), Division Newport, Newport, RI. A brief overview of the model derivation and comparisons to measured data previously appeared in a Technical Memorandum by D. McCammon and S. Hollingsworth of the Applied Research Laboratory of Pennsylvania State University.

**Associate Editor: R. Chapman.**

The author is with the Naval Undersea Warfare Center, Newport, RI 02841 USA (e-mail: cathy.clark@navy.mil).

Digital Object Identifier 10.1109/JOE.2012.2196169

A closed form for the plane-wave bottom reflection coefficient for the case of a thin elastic–solid layer over a hard basement, and an analysis of the contributions of specific families of paths through the sediment were achieved by Chapman and Chapman in 1993 [16]. The results of Chapman and Chapman were generalized in a paper by Ainslie published in 1995 [17], and Ainslie and Burns rederived the reflection and transmission coefficients with complex Lamé parameters to satisfy conservation of energy, also in 1995 [18]. Criteria for distinguishing the effects of interface waves from the excitation of propagating shear waves in the sediment were subsequently discussed by Tollefsen in conjunction with analysis of measured shallow-water data sets [19] and also by Ainslie [20].

This paper presents another derivation of a closed-form reflection coefficient which includes all paths through an elastic bottom sediment overlying a hard basement. It consolidates compressional and shear reflections and transmissions through a layered sediment into a single reflection coefficient for use in conjunction with the normal mode model described in [24]. The derivation is accomplished by formulating the various conversions as an infinite sum of matrices and expressing the result as a convergent series. The overall bottom reflection coefficient thus derived is utilized in the mode model to satisfy the bottom boundary condition in forming the modes. The motivation for the approach is the efficiency of the resultant algorithm and the ability to isolate the acoustic effects resulting from the interaction of various path types with the bottom sediment. A number of the data sets referenced above will be utilized as a means of verifying the accuracy of the model documented herein. Although the agreement with measurements is not exact, resonance effects with frequency are clearly reproduced, and the agreement is comparable to that of the other models represented. We begin with an overview of the measured data sets in Section II.

Section III presents the elastic components which are assumed to be continuous at the water/sediment and sediment/basement boundaries. Section IV includes a derivation for shear and compressional reflection and transmission coefficients at each boundary, and Section V shows a comparison of results to published curves of shear and compressional reflection and transmission coefficients as a function of grazing angle [21]–[23]. Section VI discusses the combination of the individual coefficients into a single reflection coefficient representing compressional-wave energy returning from the bottom sediment into the water column. In Section VII, the bottom reflection coefficient is utilized in the propagation model described in [24], and the results are compared to bottom

and propagation loss calculations and measured data from the references listed in Section II [3]–[26].

## II. MEASURED DATA SETS

The following data sets and references were selected because they evidence shear effects in bottom-interacting sound propagation. The data sets are described in more detail in Section VII, but a brief introductory overview is provided for the sake of clarity.

- 1) Experimental data gathered on the Scotian Shelf in 1978 in a joint program with the Applied Research Laboratory of Pennsylvania State University (Reston, VA) and the Defence Research Establishment Atlantic (DREA, Halifax, NS, Canada) is described by Beebe and Holland [3], with supporting environmental and geoaoustic parametrization provided by Beebe and McDaniel [4], [5]. The bottom for a set of measurements at a range of 8.3 km consisted of a thin sediment over granite bedrock, with high losses below 250 Hz believed to be attributable to shear losses in the granite.
- 2) In a later paper, Beebe and Holland discuss propagation effects as a function of frequency from the same data set, but at a (different) range of 4 km [6]. Beebe and Holland varied bottom parameter values to obtain a “best fit” to the data, and attributed low-frequency losses to shear effects in the sediment layer in addition to those resulting from interaction with the underlying granite.
- 3) Measurements using a bottom-mounted array on the Continental Shelf of the British Isles in the summer are documented by Ellis, Staal, and Chapman of DREA [7], [8]. The data utilized herein show resonance effects observed at a range of 55 km which are associated with acoustic interaction with a chalk bottom.
- 4) Data gathered on the Eastern Canadian Continental Shelf over a hard rock (granite) seabed are documented by Ellis, Chapman, Staal, and Hughes of DREA [9]–[12]. High losses between 10 and 100 Hz observed at a range of 13 km are believed to be the result of shear resonance effects.

## III. BOUNDARY CONDITIONS

We begin the derivation of the bottom reflection coefficient with a discussion of the boundary conditions to be satisfied. From [27, p.31, (5.1)], given the particle displacement vector  $u(x, z, t)$ , we assume the horizontal ( $x$ ) and vertical ( $z$ ) components of the stress tensor  $Z$  must be continuous at the boundary between the water and the sediment

$$\begin{aligned} Z_z &= \lambda \left( \frac{\partial u_x}{\partial x} + \frac{\partial u_z}{\partial z} \right) + 2\mu \left( \frac{\partial u_z}{\partial z} \right) \\ Z_x &= \mu \left( \frac{\partial u_x}{\partial z} + \frac{\partial u_z}{\partial x} \right) \end{aligned} \quad (1)$$

where we assume continuous propagation of a plane acoustic wave of radian frequency  $\omega$  over time; the boundary is horizontal (normal to the  $z$ -axis); the wavefronts lie in the  $xz$ -plane;  $\lambda, \mu$  are the Lamé constants, and the positive  $z$ -axis is assumed down. We also assume that the shear stress tensor vanishes in

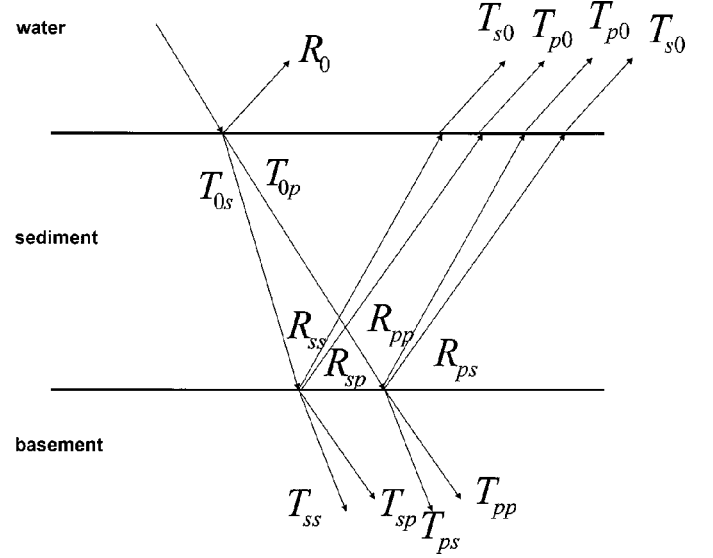


Fig. 1. Shear- and compressional-wave reflection and transmission.

the water. From [27, p. 33, (5.8)], with  $\phi$  and  $\psi$  representing compressional and shear waves, respectively, we have

$$u_x = \frac{\partial \phi}{\partial x} - \frac{\partial \psi}{\partial z}, \quad u_z = \frac{\partial \phi}{\partial z} + \frac{\partial \psi}{\partial x}. \quad (2)$$

Let  $k$  represent the horizontal wave number and  $k_z$  the vertical wave number, i.e.,

$$k_{z_p}^2 = \left( \frac{\omega}{c_p} \right)^2 - k^2 \quad \text{and} \quad k_{z_s}^2 = \left( \frac{\omega}{c_s} \right)^2 - k^2 \quad (3)$$

where  $c_p$  and  $c_s$ , the compressional and shear sound speeds, are assumed constant within layers. The compressional and shear plane waves can then be written as

$$\phi = e^{\pm i k_{z_p} z} e^{i(kx - \omega t)} \quad \text{and} \quad \psi = e^{\pm i k_{z_s} z} e^{i(kx - \omega t)}. \quad (4)$$

Through the remainder of this section, we suppress the factor  $e^{i(kx - \omega t)}$ , which is understood to multiply all of the wave functions.

The geometry for a single cycle of reflections and transmissions through a single sediment layer overlying a basement half-space is depicted in the  $xz$ -plane in Fig. 1, where the reflection and transmission coefficients are subscripted by  $p$  and  $s$  to denote compressional and shear waves, respectively, and the subscript 0 indicates reflection or transmission at the water–column interface. Since we wish to compute compressional propagation in the water, we will be concerned with the five paths propagating upward from the water/sediment boundary in Fig. 1.

To formulate the continuity conditions at the boundaries, from (1) and (2), we have

$$\begin{aligned} Z_z &= \lambda \left( \frac{\partial^2 \phi}{\partial x^2} - \frac{\partial^2 \psi}{\partial x \partial z} + \frac{\partial^2 \phi}{\partial z^2} + \frac{\partial^2 \psi}{\partial x \partial z} \right) \\ &\quad + 2\mu \left( \frac{\partial^2 \phi}{\partial z^2} + \frac{\partial^2 \psi}{\partial x \partial z} \right) \\ &= \lambda \nabla^2 \phi + 2\mu \left( \frac{\partial^2 \phi}{\partial z^2} + \frac{\partial^2 \psi}{\partial x \partial z} \right). \end{aligned} \quad (5)$$

From the wave equation

$$\nabla^2 \phi = -\frac{\omega^2}{c_p^2} \phi$$

and from (3) and (4)

$$\frac{\partial^2 \phi}{\partial z^2} = -\frac{\omega^2}{c_p^2} \phi + k^2 \phi \quad \text{and} \quad \frac{\partial^2 \psi}{\partial x \partial z} = ik \frac{\partial \psi}{\partial z}.$$

Substituting into (5) and simplifying

$$Z_z = \lambda \left( -\frac{\omega^2}{c_p^2} \right) \phi + 2\mu \left( -\frac{\omega^2}{c_p^2} \phi + k^2 \phi + ik \frac{\partial \psi}{\partial z} \right). \quad (6)$$

But

$$\lambda + 2\mu = \rho c_p^2 \quad \text{and} \quad \mu = \rho c_s^2 \quad (7)$$

where  $\rho$  is density, so we have

$$\begin{aligned} Z_z &= -\rho \omega^2 \phi + 2\rho c_s^2 k^2 \phi + 2\rho c_s^2 ik \frac{\partial \psi}{\partial z} \\ &= \rho c_s^2 (2ik) \left[ -\frac{\omega^2}{c_s^2} \frac{1}{2ik} \phi - ik \phi + \frac{\partial \psi}{\partial z} \right] \\ &= \omega^2 (2ik) \rho \frac{c_s^2}{\omega^2} \left[ \frac{\partial \psi}{\partial z} - i\phi \left( k - \frac{1}{2k} \frac{\omega^2}{c_s^2} \right) \right]. \end{aligned} \quad (8)$$

Since the factor  $\omega^2 (2ik)$  is constant over the layers and it will cancel in the reflection coefficient, it is omitted to simplify the equations. Thus, we formulate the normal stress as

$$\alpha \left( \frac{\partial \psi}{\partial z} - i\beta \phi \right) \quad (9)$$

where  $\alpha = (\rho c_s^2 / \omega^2)$  and  $\beta = k - (1/(2k))(\omega^2 / c_s^2)$ .

Similarly, from (1) and (2), we have

$$\begin{aligned} Z_x &= \mu \left( \frac{\partial^2 \phi}{\partial x \partial z} - \frac{\partial^2 \psi}{\partial z^2} + \frac{\partial^2 \phi}{\partial x \partial z} + \frac{\partial^2 \psi}{\partial x^2} \right) \\ &= \mu \left( -\frac{\partial^2 \psi}{\partial z^2} + \frac{\partial^2 \psi}{\partial x^2} + 2\frac{\partial^2 \phi}{\partial x \partial z} \right). \end{aligned} \quad (10)$$

Substituting

$$\begin{aligned} \frac{\partial^2 \psi}{\partial z^2} &= -\frac{\omega^2}{c_s^2} \psi + k^2 \psi \\ \frac{\partial^2 \psi}{\partial x^2} &= -k^2 \psi \quad \text{and} \quad \frac{\partial \phi}{\partial x \partial z} = -ik \frac{\partial \phi}{\partial z} \end{aligned}$$

into (10), we have

$$\begin{aligned} Z_x &= \rho c_s^2 \left( \frac{\omega^2}{c_s^2} \psi - 2k^2 \psi + 2ik \frac{\partial \phi}{\partial z} \right) \\ &= \rho c_s^2 (2ik) \left[ -\frac{\omega^2}{c_s^2} \frac{i}{2k} \psi + ik \psi + \frac{\partial \phi}{\partial z} \right] \\ &= \omega^2 (2ik) \frac{\rho c_s^2}{\omega^2} \left[ \frac{\partial \phi}{\partial z} + i\psi \left( k - \frac{\omega^2}{c_s^2} \frac{1}{2k} \right) \right]. \end{aligned}$$

Again, the factor  $\omega^2 (2ik)$  may be neglected, and we formulate the tangential stress as

$$\alpha \left( \frac{\partial \phi}{\partial z} + i\beta \psi \right) \quad (11)$$

with  $\alpha$  and  $\beta$  defined as in (9).

From (2), the conditions for horizontal and vertical displacement or continuity of  $u_x$  and  $u_z$  are simply

$$\frac{\partial \psi}{\partial z} - ik\phi \quad \text{and} \quad \frac{\partial \phi}{\partial z} + ik\psi$$

since  $\partial \phi / \partial x = ik\phi$  and  $\partial \psi / \partial x = ik\psi$ .

To summarize, for the water/sediment interface, the three boundary conditions, normal stress, vertical displacement, and tangential stress are expressed as continuity of the quantities

$$\alpha \left( \frac{\partial \psi}{\partial z} - i\beta \phi \right), \quad \frac{\partial \phi}{\partial z} + ik\psi, \quad \text{and} \quad \alpha \left( \frac{\partial \phi}{\partial z} + i\beta \psi \right) \quad (12)$$

respectively, with  $\alpha$  and  $\beta$  as in (9). The boundary at the sediment/basement interface also requires continuity of horizontal displacement

$$\frac{\partial \psi}{\partial z} - ik\phi \quad (13)$$

in addition to the conditions in (12).

#### IV. REFLECTION AND TRANSMISSION COEFFICIENTS

To derive the reflection and transmission coefficients at each boundary, consider the functions depicted in Fig. 2, i.e., let the compressional-wave function in the water be given by

$$\phi_0 = A_0 e^{ik_{z_0} z} + B_0 e^{-ik_{z_0} z} \quad (14)$$

and let the compressional- and shear-wave functions in the sediment layer be given by

$$\phi_1 = A e^{ik_{z_{p1}} z} + B e^{-ik_{z_{p1}} z} \quad \text{and} \quad \psi_1 = C e^{ik_{z_{s1}} z} + D e^{-ik_{z_{s1}} z} \quad (15)$$

respectively, and let the compressional- and shear-wave functions in the basement be given by

$$\phi_2 = E e^{ik_{z_{p2}} z} + F e^{-ik_{z_{p2}} z} \quad \text{and} \quad \psi_2 = G e^{ik_{z_{s2}} z} + H e^{-ik_{z_{s2}} z} \quad (16)$$

respectively, where  $k_z = \sqrt{(\omega/c)^2 - k^2}$  represents vertical wave number for radian frequency  $\omega$  and sound speed  $c$ , and depth  $z$  is positive down.

We will treat each of three sets of conditions separately: (A) reflection and transmission of the incident wave at the water/sediment interface; (B) transmission of the reflected waves from the sediment layer into the water column; and (C) reflection and transmission of the waves at the sediment/basement interface, as depicted in Fig. 3. For now, each interface will be taken to occur at  $z = 0$ .

It should be noted that the effects of both compressional- and shear-wave attenuations are represented in the model by an imaginary component of wave number, i.e., all calculations discussed below are performed using complex arithmetic with  $\text{Im}(k) = \ln(10^{a.f/20})$ , where  $a$  is the appropriate loss in decibels per unit distance and  $f$  is frequency in kilohertz.

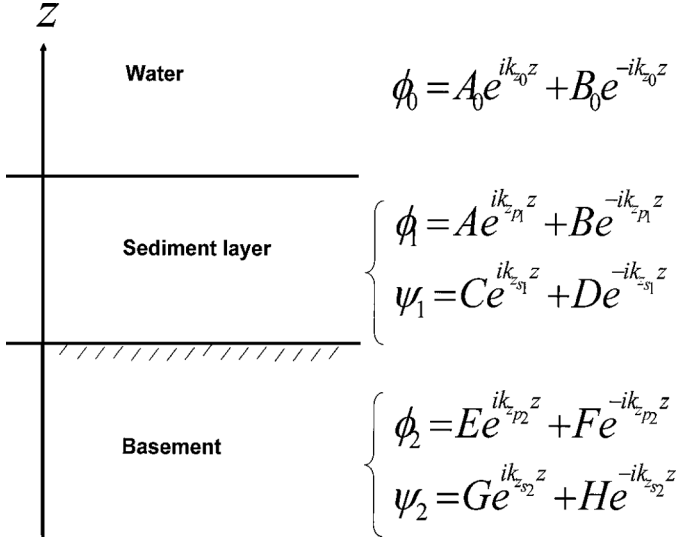


Fig. 2. Shear- and compressional-wave functions.

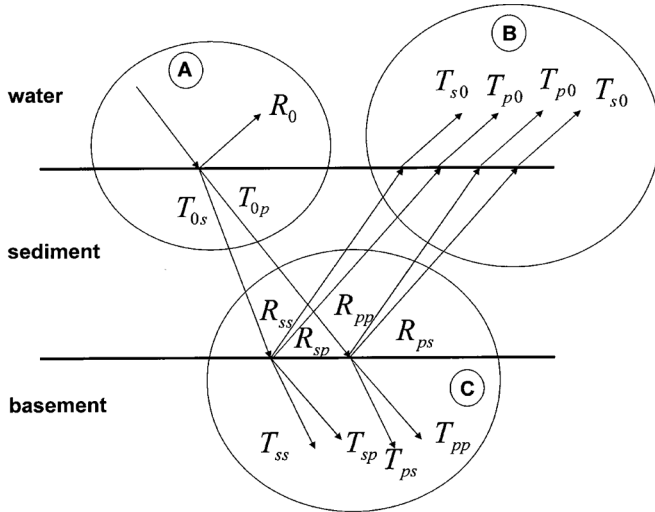


Fig. 3. Depiction of three sets of reflection and transmission coefficients.

### A. Water/Sediment Coefficients

For the water/sediment interface, we have

$$\alpha_0 \beta_0 = \rho_0 \frac{c_{s_0}^2}{\omega^2} \left( k - \frac{1}{2k} \frac{\omega^2}{c_{s_0}^2} \right) = \frac{\rho_0 c_{s_0}^2 k}{\omega^2} - \frac{\rho_0}{2k}.$$

In the limit, since  $c_{s_0} = 0$ , we use  $\alpha_0 \beta_0 = -(\rho_0/(2k))$ . Referring to the wave functions defined in Fig. 2, the first boundary condition in (12) is

$$-i\alpha_0 \beta_0 \phi_0 = \alpha_1 \left( \frac{\partial \psi_1}{\partial z} - i\beta \phi_1 \right).$$

Thus, assuming  $\rho_0 = 1$ ,  $\psi_0 = 0$ , and  $c_{s_0} = 0$ , the boundary conditions for this case are

$$\begin{cases} \phi_0 = 2k\alpha_1 \left( -i \frac{\partial \psi_1}{\partial z} - \beta_1 \phi_1 \right) \\ \frac{\partial \phi_0}{\partial z} = \frac{\partial \phi_1}{\partial z} + ik\psi_1 \\ \frac{\partial \phi_1}{\partial z} + i\beta_1 \psi_1 = 0 \end{cases} \quad (17)$$

where  $\alpha_i = (\rho_i c_{s_i}^2)/\omega^2$  and  $\beta_i = k - (1/(2k))(\omega^2/c_{s_i}^2)$  as above. Letting  $z = 0$  at the interface, (17) becomes

$$\begin{cases} A_0 + B_0 = 2k\alpha_1 [k_{z_{s1}}(C - D) - \beta_1(A + B)] \\ k_{z_0}(A_0 - B_0) = k_{p_1}(A - B) + k(C + D) \\ k_{z_{p1}}(A - B) + \beta_1(C + D) = 0. \end{cases} \quad (18)$$

Now let  $A_0 = R_0$ ,  $B_0 = 1$ ,  $A = 0$ ,  $B = T_{0p}$ ,  $C = 0$ , and  $D = T_{0s}$ . Then, we have

$$\begin{cases} R_0 + 1 = 2k\alpha_1 [-k_{z_{s1}}T_{0s} - \beta_1 T_{0p}] \\ k_{z_0}(R_0 - 1) = -k_{z_{p1}}T_{0p} + kT_{0s} \\ -k_{z_{p1}}T_{0p} + \beta_1 T_{0s} = 0. \end{cases}$$

Solving for  $T_{0p}$  in the last equation and substituting into the first two yields

$$1 + R_0 = -2k\alpha_1 \left( k_{z_{s1}} + \frac{\beta_1^2}{k_{z_{p1}}} \right) T_{0s}$$

and

$$1 - R_0 = \frac{\beta_1 - k}{k_{z_0}} T_{0s}.$$

Adding the two equations, we have

$$2 = \left[ -2k\alpha_1 \left( k_{z_{s1}} + \frac{\beta_1^2}{k_{z_{p1}}} \right) + \frac{\beta_1 - k}{k_{z_0}} \right] T_{0s}.$$

Solving for  $T_{0s}$  yields

$$T_{0s} = \frac{-2}{2k\alpha_1 \left( k_{z_{s1}} + \frac{\beta_1^2}{k_{z_{p1}}} \right) + \frac{k - \beta_1}{k_{z_0}}}.$$

Using this result to solve for the remaining coefficients, we have

$$T_{0p} = \frac{\frac{-2\beta_1}{k_{z_{p1}}}}{2k\alpha_1 \left( k_{z_{s1}} + \frac{\beta_1^2}{k_{z_{p1}}} \right) + \frac{k - \beta_1}{k_{z_0}}}$$

and

$$R_0 = \frac{2k\alpha_1 \left( k_{z_{s1}} + \frac{\beta_1^2}{k_{z_{p1}}} \right) + \frac{\beta_1 - k}{k_{z_0}}}{2k\alpha_1 \left( k_{z_{s1}} + \frac{\beta_1^2}{k_{z_{p1}}} \right) + \frac{k - \beta_1}{k_{z_0}}}.$$

### B. Sediment/Water Coefficients

Expanding the (B) section of Fig. 3, we define four reflection coefficients as depicted in Fig. 4.

To derive the coefficients identified in Fig. 4(a), let  $A_0 = T_{s0}$ ,  $B_0 = 0$ ,  $A = 0$ ,  $B = R_{sp0}$ ,  $C = 1$ , and  $D = R_{ss0}$ . The boundary conditions in (18) become

$$\begin{cases} T_{s0} = 2k\alpha_1 [k_{z_{s1}}(1 - R_{ss0}) - \beta_1 R_{sp0}] \\ k_{z_0} T_{s0} = -k_{z_{p1}} R_{sp0} + k(1 + R_{ss0}) \\ -k_{z_{p1}} R_{sp0} + \beta_1(1 + R_{ss0}) = 0. \end{cases}$$

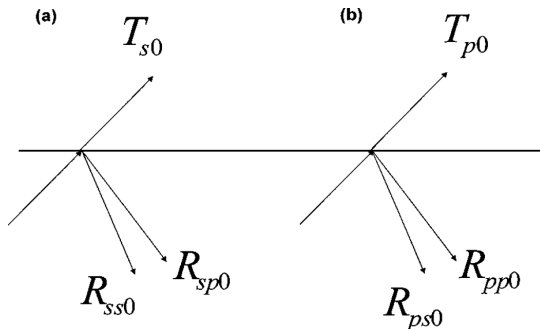


Fig. 4. Sediment/water reflection and transmission coefficients.

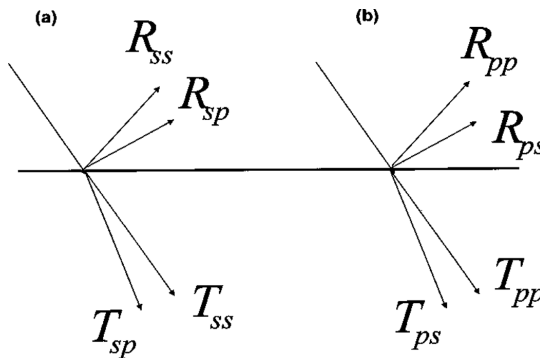


Fig. 5. Sediment/basement reflection and transmission coefficients.

Solving for  $R_{sp0}$  in the last equation and substituting into the first two yields

$$T_{s0} = 2k\alpha_1 \left[ k_{z_{s1}}(1 - R_{ss0}) - \frac{\beta_1^2}{k_{z_{p1}}}(1 + R_{ss0}) \right]$$

and

$$T_{s0} = \frac{k - \beta_1}{k_{z_0}}(1 + R_{ss0}).$$

Subtracting the two equations and solving for  $R_{ss0}$ , we have

$$R_{ss0} = \frac{2k\alpha_1 \left( k_{z_{s1}} - \frac{\beta_1^2}{k_{z_{p1}}} \right) + \frac{\beta_1 - k}{k_{z_0}}}{2k\alpha_1 \left( k_{z_{s1}} + \frac{\beta_1^2}{k_{z_{p1}}} \right) + \frac{k - \beta_1}{k_{z_0}}}. \quad (19)$$

Solving for the remaining coefficients gives

$$R_{sp0} = \frac{4k\alpha_1\beta_1 \frac{k_{z_{s1}}}{k_{z_{p1}}}}{2k\alpha_1 \left( k_{z_{s1}} + \frac{\beta_1^2}{k_{z_{p1}}} \right) + \frac{k - \beta_1}{k_{z_0}}}$$

and

$$T_{s0} = \frac{4k\alpha_1 k_{z_{s1}} \frac{k - \beta_1}{k_{z_0}}}{2k\alpha_1 \left( k_{z_{s1}} + \frac{\beta_1^2}{k_{z_{p1}}} \right) + \frac{k - \beta_1}{k_{z_0}}}.$$

Similarly, to derive the coefficients identified in Fig. 4(b), let  $A_0 = T_{p0}$ ,  $B_0 = 0$ ,  $A = 1$ ,  $B = R_{pp0}$ ,  $C = 0$ , and  $D = R_{ps0}$ .

The boundary conditions in (18) become

$$\begin{cases} T_{p0} = 2k\alpha_1 [-k_{z_{s1}} R_{ps0} - \beta_1(1 + R_{pp0})] \\ k_{z_0} T_{p0} = k_{z_{p1}}(1 - R_{pp0}) + k R_{ps0} \\ k_{z_{p1}}(1 - R_{pp0}) + \beta_1 R_{ps0} = 0. \end{cases}$$

Substituting the solution for  $R_{ps0}$  in the last equation into the first two and combining the results gives

$$R_{pp0} = \frac{2k\alpha_1 \left( k_{z_{s1}} - \frac{\beta_1^2}{k_{z_{p1}}} \right) + \frac{k - \beta_1}{k_{z_0}}}{2k\alpha_1 \left( k_{z_{s1}} + \frac{\beta_1^2}{k_{z_{p1}}} \right) + \frac{k - \beta_1}{k_{z_0}}}.$$

Solving for the remaining coefficients, we have

$$R_{ps0} = \frac{-4k\alpha_1\beta_1}{2k\alpha_1 \left( k_{z_{s1}} + \frac{\beta_1^2}{k_{z_{p1}}} \right) + \frac{k - \beta_1}{k_{z_0}}}$$

and

$$T_{p0} = \frac{4k\alpha_1\beta_1 \frac{\beta_1 - k}{k_{z_0}}}{2k\alpha_1 \left( k_{z_{s1}} + \frac{\beta_1^2}{k_{z_{p1}}} \right) + \frac{k - \beta_1}{k_{z_0}}}.$$

### C. Sediment/Basement Coefficients

Expanding the (C) section of Fig. 3, we define eight reflection coefficients as depicted in Fig. 5. In this case, we require a fourth boundary condition, i.e., we assume continuity of all the boundary conditions in (12) and (13).

To derive the coefficients identified in Fig. 5(a), with reference to the wave functions defined in Fig. 2, let  $A = R_{sp}$ ,  $B = 0$ ,  $C = R_{ss}$ ,  $D = 1$ ,  $E = 0$ ,  $F = T_{sp}$ ,  $G = 0$ , and  $H = T_{ss}$ . Letting  $(\alpha_2/\alpha_1) = \gamma$ , the four equations in (12) and (13) become

$$\begin{aligned} k_{z_{s1}}(R_{ss} - 1) - \beta_1 R_{sp} &= \gamma(-k_{z_{s2}} T_{ss} - \beta_2 T_{sp}) \\ k_{z_{p1}} R_{sp} + k(1 + R_{ss}) &= -k_{z_{p2}} T_{sp} + k T_{ss} \\ k_{z_{p1}} R_{sp} + \beta_1(R_{ss} + 1) &= \gamma(-k_{z_{p2}} T_{sp} + \beta_2 T_{ss}) \\ k_{z_{s1}}(R_{ss} - 1) - k R_{sp} &= -k_{z_{s2}} T_{ss} - k T_{sp}. \end{aligned} \quad (20)$$

For simplicity of notation, let

$$\begin{aligned} x_1 &= (k - \gamma\beta_2)k_{z_{p1}} + (k\gamma - \beta_1)k_{z_{p2}} \\ x_2 &= (k - \gamma\beta_2)k_{z_{s1}} + (k\gamma - \beta_1)k_{z_{s2}} \\ x_3 &= k_{z_{s2}}k_{z_{p1}}(1 - \gamma) - k(\gamma\beta_2 - \beta_1) \\ x_4 &= k_{z_{p2}}k_{z_{s1}}(1 - \gamma) - k(\gamma\beta_2 - \beta_1) \\ x_5 &= k(\gamma\beta_2 - \beta_1). \end{aligned} \quad (21)$$

Solving (20) yields

$$R_{ss} = \frac{(k_{z_{s1}}k_{z_{p2}}(1 - \gamma) + x_5)x_3 + (k_{z_{s1}}(k - \gamma\beta_2) - k_{z_{s2}}(k\gamma - \beta_1))x_1}{x_1x_2 + x_3x_4}$$

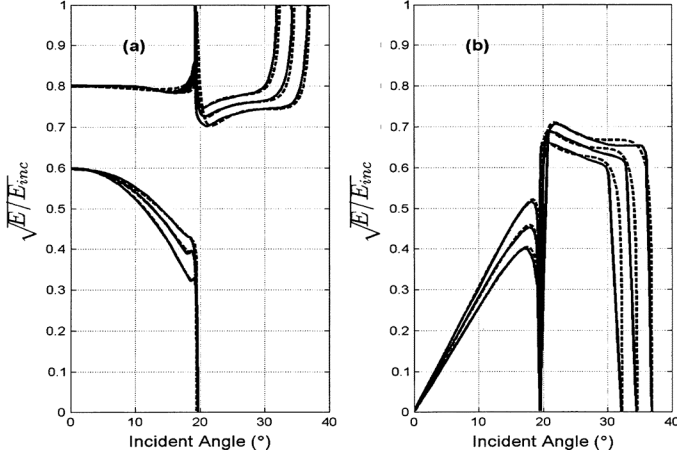


Fig. 6. Water/sediment coefficients: (a)  $R_0$  and  $T_{0p}$  (see [21, Figs. 3–7, p. 82]); (b)  $T_{0s}$  (see [21, Figs. 3–8, p. 82]).

TABLE I  
INPUTS FOR FIGS. 6–9

Figure	$\rho_1/\rho_0$	$c_{p1}/c_0$	$c_{p1}/c_{s1}$
7	3	3	1.6, 1.7, 1.8
8, 10(a)	1/3	5	1.6, 1.7, 1.8
9, 10(b)	1/3	5	1.6, 1.7, 1.75

TABLE II  
INPUTS FOR FIGS. 10–12

	$\rho_2/\rho_1$	$c_{p2}/c_{p1}$	$c_{p1}/c_{s1}$	$c_{s2}/c_{s1}$
1	1.036	1.07	1.7097	1.07
2	1.09	1.10	1.7321	1.09
3	1	1.14	1.8091	1.30
4	1.103	1.286	1.7321	1.286

$$\begin{aligned}
 R_{sp} &= \frac{2k_{z_{s1}} \left( (k - \gamma\beta_2)x_5 + k_{z_{s2}} k_{z_{p2}} (1 - \gamma)(k\gamma - \beta_1) \right)}{x_1x_2 + x_3x_4} \\
 T_{ss} &= \frac{-2k_{z_{s1}} (\beta_1 - k) \left( k_{z_{p1}} (k - \gamma\beta_2) + k_{z_{p2}} (k\gamma - \beta_1) \right)}{x_1x_2 + x_3x_4} \\
 T_{sp} &= \frac{2k_{z_{s1}} (\beta_1 - k)x_3}{x_1x_2 + x_3x_4}. \tag{22}
 \end{aligned}$$

Similarly, to solve for the coefficients in Fig. 5(b), let  $A = R_{pp}$ ,  $B = 1$ ,  $C = R_{ps}$ ,  $D = 0$ ,  $E = 0$ ,  $F = T_{pp}$ ,  $G = 0$ , and  $H = T_{ps}$ , the four equations in (12) and (13), become

$$\begin{aligned}
 k_{z_{s1}} R_{ps} - \beta_1 (R_{pp} + 1) &= \gamma (-k_{z_{s2}} T_{ps} - \beta_2 T_{pp}) \\
 k_{z_{p1}} (R_{pp} - 1) + k R_{ps} &= -k_{z_{p2}} T_{pp} + k T_{ps} \\
 k_{z_{p1}} (R_{pp} - 1) + \beta_1 R_{ps} &= \gamma (-k_{z_{p2}} T_{pp} + \beta_2 T_{ps}) \\
 k_{z_{s1}} R_{ps} - k (R_{pp} + 1) &= -k_{z_{s2}} T_{ps} - k T_{pp}. \tag{23}
 \end{aligned}$$

Solving (23), we have

$$R_{pp} = \frac{\left( (k - \gamma\beta_2)k_{z_{p1}} - (k\gamma - \beta_1)k_{z_{p2}} \right) x_2 + k_{z_{s2}} k_{z_{p1}} (1 - \gamma) + x_4 x_5}{x_1 x_2 + x_3 x_4}$$

$$\begin{aligned}
 R_{ps} &= \frac{2k_{z_{p1}} \left( -k_{z_{p2}} k_{z_{s2}} (1 - \gamma)(k\gamma - \beta_1) - (k - \gamma\beta_2)x_5 \right)}{x_1 x_2 + x_3 x_4} \\
 T_{pp} &= \frac{-2(\beta_1 - k)k_{z_{p1}} x_2}{x_1 x_2 + x_3 x_4} \\
 T_{ps} &= \frac{-2(\beta_1 - k)k_{z_{p1}} x_4}{x_1 x_2 + x_3 x_4}. \tag{24}
 \end{aligned}$$

## V. VERIFICATION OF WATER/SEDIMENT/BASEMENT BOUNDARY COEFFICIENTS

To verify the accuracy of the reflection and transmission coefficients derived in Section IV, we compare the values as a function of incident angle to plots provided by [22] and [23] as reproduced in [21]. The inputs for three cases shown in Figs. 6–9 are provided in Table I and the inputs for the four cases shown in Figs. 10–12 are given in Table II. The reference solutions are indicated by solid lines and the model results by dashed lines. Since the reference solutions are expressed as square roots of energy ratios, the model results, which are computed as pressure ratios in the absence of absorption, are multiplied by an appropriate ratio of the form

$$\sqrt{\frac{\rho_j \tan \theta_j}{\rho_i \tan \theta_i}}$$

where  $i$  indicates the medium and type of the incident wave and  $j$  the medium and type of the reflected or transmitted wave (see [21, p. 81]). For example, denoting energy by  $E$ , the conversion of  $T_{0p}$  to energy units is

$$\sqrt{\frac{E}{E_{\text{inc}}}} = \sqrt{\frac{\rho_1 \tan \theta_{p1}}{\rho_0 \tan \theta_0}} T_{0p}$$

since it represents transmission of compressional waves in the water to compressional waves in the sediment. The conversion of  $T_{sp}$  is given by

$$\sqrt{\frac{E}{E_{\text{inc}}}} = \sqrt{\frac{\rho_2 \tan \theta_{p2}}{\rho_1 \tan \theta_{s1}}} T_{sp}$$

since it represents transmission of shear waves in the sediment to compressional waves in the basement. The agreement between the model and reference solutions is generally good, although differences in Figs. 11 and 12 for the curves which correspond to the fourth set of inputs in Table II suggest a possible discrepancy in the inputs for that case.

## VI. TOTAL REFLECTION COEFFICIENT

With reference to Fig. 1, if we trace from the incident path to each of the five compressional waves which reenter the water

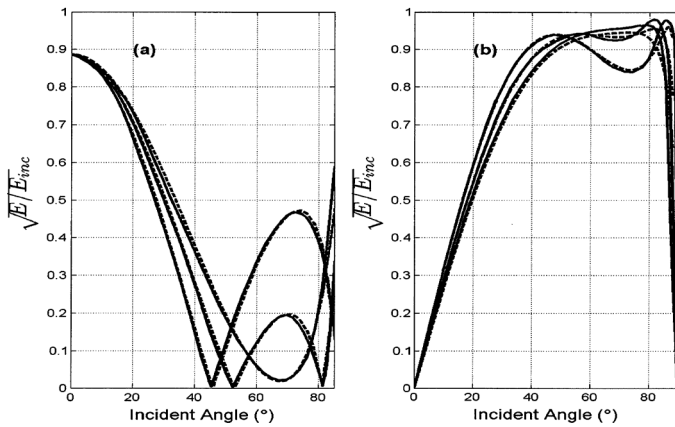


Fig. 7. Sediment/water reflection coefficients for incident compressional wave: (a)  $R_{pp0}$  (see [21, Figs. 3–9, p. 83]); (b)  $R_{ps0}$  (see [21, Figs. 3–10, p. 84]).

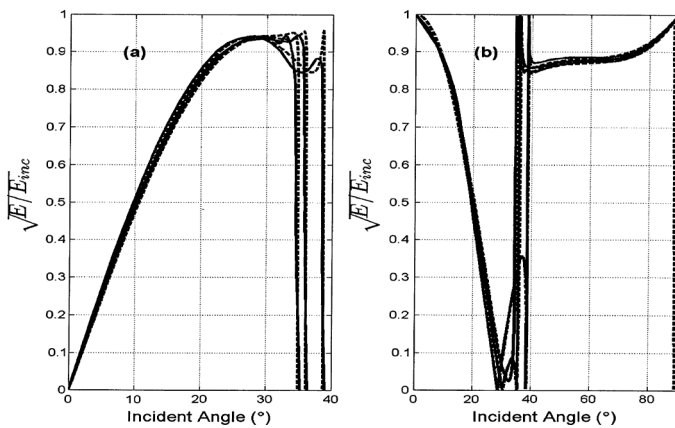


Fig. 8. Sediment/water reflection coefficients for incident shear wave: (a)  $R_{sp0}$  (see [21, Figs. 3–13, p. 86]); (b)  $R_{ss0}$  (see [21, Figs. 3–12, p. 85]).

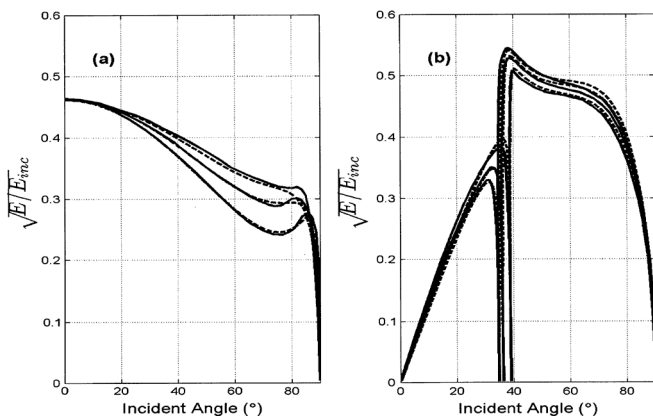


Fig. 9. Sediment/water transmission coefficients: (a)  $T_{p0}$  (see [21, Figs. 3–11, p. 85]); (b)  $T_{s0}$  (see [21, Figs. 3–14, p. 86]).

column, we see that including only the zeroth-order terms in the overall reflection coefficient  $R$ , we have

$$R = R_0 + T_{0p}R_{pp}T_{p0} + T_{0p}R_{ps}T_{s0} + T_{0s}R_{sp}T_{p0} + T_{0s}R_{ss}T_{s0}. \quad (25)$$

To clarify, the compressional wave emerging back into the water column consists of components associated with each of the terms in (25) which correspond to reflection from the water/sediment interface ( $R_0$ ), compressional transmission into

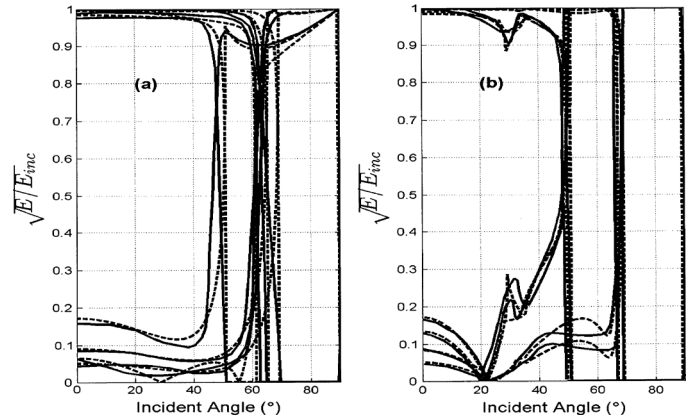


Fig. 10. Sediment/basement coefficients: (a)  $R_{pp}, T_{pp}$  (see [21, Figs. 3–15(a), p. 88]); (b)  $R_{ss}, T_{ss}$  (see [21, Figs. 3–15(c), p. 88]).

the sediment followed by compressional basement reflection and then transmission back into the water ( $T_{0p}R_{pp}T_{p0}$ ), etc. Each of the reflection and transmission coefficients below the water/sediment interface is understood to include a suppressed phase term. If a subscript ends in  $p$ , the suppressed phase term is  $e^{ik_{zp_1}d_1}$ , where  $d_1$  is the layer thickness. Likewise, if a subscript ends in  $s$ , the suppressed phase term is  $e^{ik_{zs_1}d_1}$ . For example,  $T_{0p}$  is actually  $T_{0p}e^{ik_{zp_1}d_1}$  and  $T_{0p}R_{pp}T_{p0}$  is  $T_{0p}R_{pp}T_{p0}e^{2ik_{zp_1}d_1}$ , etc.

We represent (25) in matrix form as

$$R = R_0 + (T_{0p} \ T_{0s}) \begin{pmatrix} R_{pp} & R_{ps} \\ R_{sp} & R_{ss} \end{pmatrix} \begin{pmatrix} T_{p0} \\ T_{s0} \end{pmatrix}. \quad (26)$$

The effect of an additional cycle within the sediment as depicted in Fig. 13 can be written in matrix form as

$$X = \begin{pmatrix} R_{pp0} & R_{ps0} \\ R_{sp0} & R_{ss0} \end{pmatrix} \begin{pmatrix} R_{pp} & R_{ps} \\ R_{sp} & R_{ss} \end{pmatrix} \quad (27)$$

where the suppressed phase terms are assumed. Thus, the 16 first-order terms of the reflection coefficient are

$$(T_{0p} \ T_{0s}) \begin{pmatrix} R_{pp} & R_{ps} \\ R_{sp} & R_{ss} \end{pmatrix} X \begin{pmatrix} T_{p0} \\ T_{s0} \end{pmatrix} \quad (28)$$

and the terms of the  $n$ th order are

$$(T_{0p} \ T_{0s}) \begin{pmatrix} R_{pp} & R_{ps} \\ R_{sp} & R_{ss} \end{pmatrix} X^n \begin{pmatrix} T_{p0} \\ T_{s0} \end{pmatrix}. \quad (29)$$

Including all cycles, the total reflection coefficient is given by

$$R = R_0 + (T_{0p} \ T_{0s}) \begin{pmatrix} R_{pp} & R_{ps} \\ R_{sp} & R_{ss} \end{pmatrix} \sum_{n=0}^{\infty} X^n \begin{pmatrix} T_{p0} \\ T_{s0} \end{pmatrix} \quad (30)$$

if the infinite series converges, which it will under normal conditions, as shown in [28]. The details of the proof are repeated here in the Appendix.

A closed-form expression for  $R$  is obtained by diagonalizing the matrix  $X$ . The eigenvalues of  $X$  are the solutions of

$$|X - \lambda I| = 0.$$

Letting

$$X = \begin{pmatrix} x_{11} & x_{12} \\ x_{21} & x_{22} \end{pmatrix}$$

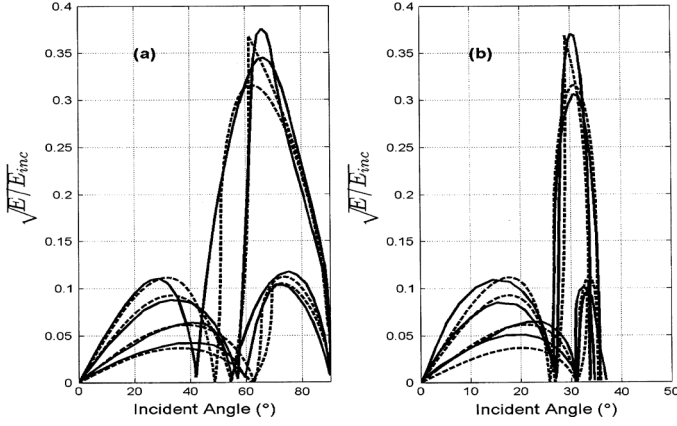


Fig. 11. Sediment/basement reflection coefficients: (a)  $R_{ps}$  (see [21, Figs. 3–16(a), p. 89]); (b)  $R_{sp}$  (see [21, Figs. 3–16(e), p. 89]).

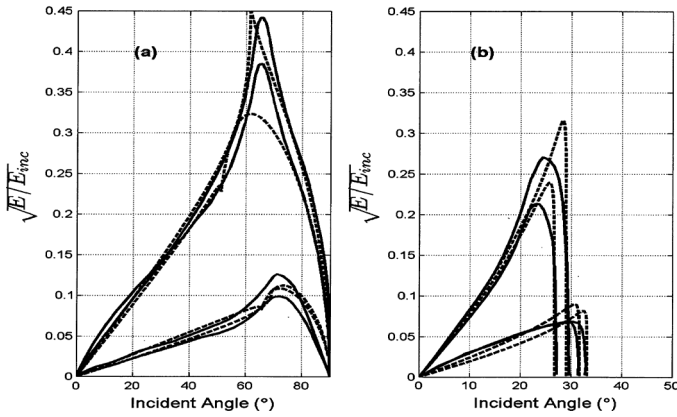


Fig. 12. Sediment/basement transmission coefficients: (a)  $T_{ps}$  (see [21, Figs. 3–16(b), p. 89]); (b)  $T_{sp}$  (see [21, Figs. 3–16(h), p. 89]).

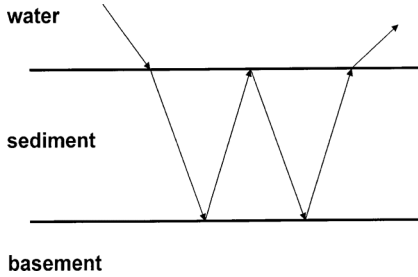


Fig. 13. Depiction of a single additional sediment cycle.

the eigenvalues are

$$\lambda_1 = \frac{x_{11} + x_{22} + \sqrt{(x_{11} - x_{22})^2 + 4x_{12}x_{21}}}{2}$$

$$\lambda_2 = \frac{x_{11} + x_{22} - \sqrt{(x_{11} - x_{22})^2 + 4x_{12}x_{21}}}{2}. \quad (31)$$

The matrix  $X$  is diagonalized by finding the two eigenvectors  $E_1$  and  $E_2$  such that

$$XE_1 = \lambda_1 E_1$$

$$XE_2 = \lambda_2 E_2$$

and forming the matrix whose columns are  $E_1$  and  $E_2$

$$P = \begin{pmatrix} x_{12} & x_{12} \\ \lambda_1 - x_{11} & \lambda_2 - x_{11} \end{pmatrix}$$

Then

$$P^{-1} = \frac{1}{x_{12}(\lambda_2 - \lambda_1)} \begin{pmatrix} \lambda_2 - x_{11} & -x_{12} \\ -(\lambda_1 - x_{11}) & x_{12} \end{pmatrix}$$

and

$$P^{-1}XP = \begin{pmatrix} \lambda_1 & 0 \\ 0 & \lambda_2 \end{pmatrix} = D$$

or

$$X = PDP^{-1}.$$

Then

$$X^n = PD^nP^{-1} = P \begin{pmatrix} \lambda_1^n & 0 \\ 0 & \lambda_2^n \end{pmatrix} P^{-1}.$$

Writing the sums in closed form, we replace  $\sum_{n=0}^{\infty} X^n$  in (30) by

$$P \begin{pmatrix} \frac{1}{1 - \lambda_1} & 0 \\ 0 & \frac{1}{1 - \lambda_2} \end{pmatrix} P^{-1}. \quad (32)$$

Since all the elements of the matrices in (30) can be written in terms of the reflection coefficients derived above, we may write  $R$  in a more convenient form by letting

$$Y = \begin{pmatrix} R_{pp} & R_{ps} \\ R_{sp} & R_{ss} \end{pmatrix} P \begin{pmatrix} \frac{1}{1 - \lambda_1} & 0 \\ 0 & \frac{1}{1 - \lambda_2} \end{pmatrix} P^{-1}. \quad (33)$$

By denoting the elements of  $Y$  by

$$Y = \begin{pmatrix} y_{pp} & y_{ps} \\ y_{sp} & y_{ss} \end{pmatrix} \quad (34)$$

and expanding (33), we have

$$y_{pp} = (R_{pp} + R_{ps}R_{ss0}R_{sp} - R_{pp}R_{ss0}R_{ss})/\text{Den}$$

$$y_{ps} = (R_{ps} + R_{pp}R_{ps0}R_{ss} - R_{ps}R_{ps0}R_{sp})/\text{Den}$$

$$y_{sp} = (R_{sp} + R_{ss}R_{sp0}R_{pp} - R_{sp}R_{sp0}R_{ps})/\text{Den}$$

$$y_{ss} = (R_{ss} + R_{sp}R_{pp0}R_{ps} - R_{ss}R_{pp0}R_{pp})/\text{Den}$$

where

$$\text{Den} = 1 - R_{pp0}R_{ps}R_{ss0}R_{sp} - R_{ps0}R_{ss}R_{sp0}R_{pp}$$

$$- R_{pp0}R_{pp} - R_{ps0}R_{sp} + R_{ps0}R_{sp}R_{sp0}R_{ps}$$

$$- R_{sp0}R_{ps} - R_{ss0}R_{ss} + R_{pp0}R_{pp}R_{ss0}R_{ss}.$$

To relate these terms back to the geometry of sediment paths, we substitute (33) and (34) into (30) to obtain

$$R = R_0 + (T_{0p} \ T_{0s}) \begin{pmatrix} y_{pp} & y_{ps} \\ y_{sp} & y_{ss} \end{pmatrix} \begin{pmatrix} T_{p0} \\ T_{s0} \end{pmatrix}$$

$$= R_0 + T_{0p}y_{pp}T_{p0} + T_{0p}y_{ps}T_{s0}$$

$$+ T_{0s}y_{sp}T_{p0} + T_{0s}y_{ss}T_{s0}. \quad (35)$$

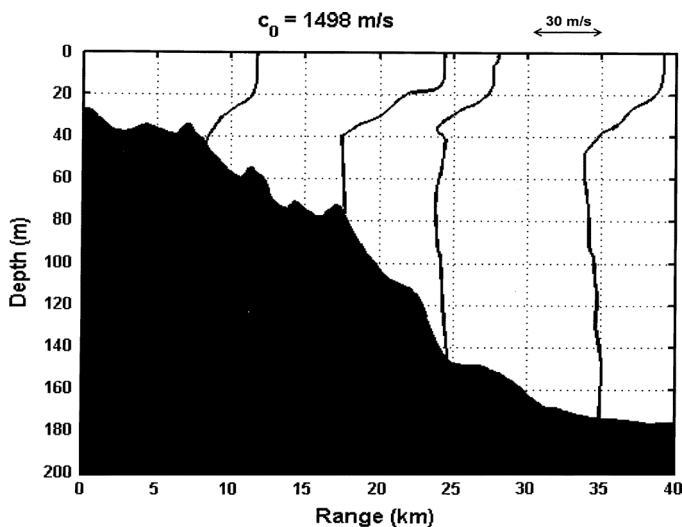


Fig. 14. Sound-speed variation and bathymetry for data sets 1 and 2.

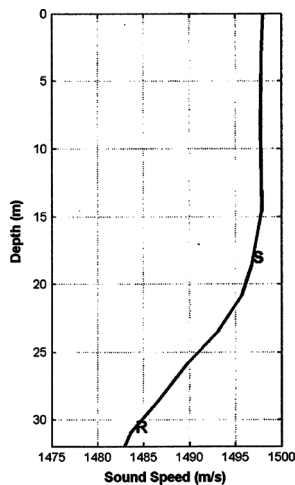


Fig. 15. Modeled sound-speed profile for data sets 1 and 2; *S* and *R* denote source and receiver, respectively.

The second term corresponds to reflected paths in the sediment which begin and end as compressional waves and the remaining terms likewise correspond to waves which convert from compressional to shear, shear to compressional, and those which begin and end as shear waves, respectively. In the model, this method of representing the total reflection coefficient enables study of the effect of individual mode types by zeroing the appropriate elements of the  $X$  array.

## VII. PROPAGATION LOSS PREDICTIONS

The ability of the mode model of [24] to reproduce known propagation effects as a function of frequency when coupled with the bottom model described herein is demonstrated through calculations involving the four data sets listed in Section II. Propagation loss for 1/3-octave broadband data is computed at the 1/3-octave center frequencies.

### A. Data Set 1

The first data set is from a set of experiments performed on the Scotian Shelf in 1978 during a joint program of the Applied Research Laboratory of Pennsylvania State University and DREA.

TABLE III  
MODELED SOUND-SPEED PROFILE FOR DATA SETS 1 AND 2

Depth (m)	Sound speed (m/s)
0	1498.00
3.18	1497.79
8.40	1497.73
14.53	1497.72
18.60	1496.74
20.86	1495.66
23.56	1492.99
25.80	1489.80
28.71	1486.43
30.96	1483.59
33.89	1481.62
36.82	1480.01
39.30	1478.22
42.92	1477.13

The example is site 2 as described by Beebe and Holland [3], with supporting environmental and geoacoustic parametrization provided by Beebe and McDaniel [4], [5]. The bottom consisted of a thin sediment layer over granite bedrock. The receiver was a vertical line array in a 32-m water column and the measurements in question were received on the bottom hydrophone of the array at a depth of 1 m above the bottom. Explosive sources were placed at various depths depending on the bathymetry. Sound-speed variation and bathymetry for the highly range-dependent environment are shown in Fig. 14. The origin of the range axis is at the receiver position.

The data we consider were recorded for a source at 8.3 km from the receiver and reference to Fig. 14 reveals that the bottom was relatively flat for ranges within about 10 km of the receive array and only a single sound-speed profile is shown within that range. Thus, we model a flat bottom at a depth of 32 m, and the single sound-speed profile is shown in Fig. 15, with source and receiver depths of 18 and 30.5 m depicted by *S* and *R*, respectively. The sound-speed and depth values used in the model are shown in Table III and the bottom parameters are summarized in Table IV.

A comparison of model results and the Beebe and Holland prediction to measured propagation loss from a source at 8.3-km range are shown in Fig. 16. Bottom interaction is significant due to the downward-refracting sound-speed profile, and the increasing loss with decreasing frequency below 250 Hz, believed to be a result of shear conversion at the basement, is reproduced by the model(s).

### B. Data Set 2

The second data set is taken from the same set of experiments as the first, i.e., the data were collected using a vertical line array on the Scotian Shelf in 1978 during a joint program of the Applied Research Laboratory of Pennsylvania State University and DREA [6]. The modeled sound speed and bathymetry, which are the same as data set 1, are shown in Fig. 15 and Table III. Source and receiver depths are 18 and 30.5 m, respectively, and the range between source and receiver is 4 km. The modeled bottom parameters, which vary from those of data set 1, are listed in Table V. The values in Table V were obtained by Beebe and Holland by a “best fit” procedure using the measured data, which is described in [6].

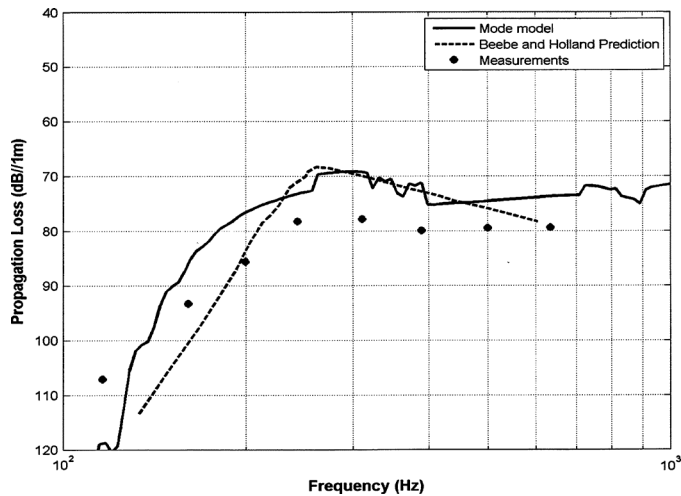


Fig. 16. Model comparison to measured propagation and viscoelastic sediment model used by Beebe and Holland to 8.3 km on the Scotian Shelf [3] (data set 1).

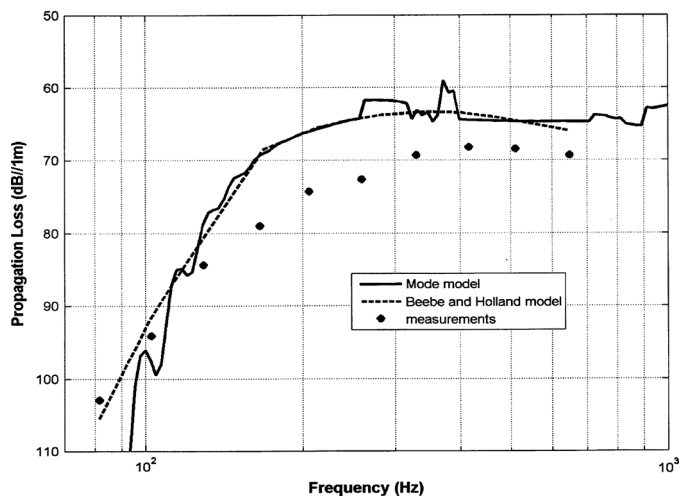


Fig. 17. Model comparison to measured propagation and Beebe and Holland prediction to 4 km on the Scotian Shelf (data set 2).

A comparison of results to propagation loss measurements and the Beebe and Holland model prediction for a solid sediment model is shown in Fig. 17.

### C. Data Set 3

The third data set involves measurements taken at a range of 55 km using a bottom-mounted array on the Continental Shelf of the British Isles in the summer in a 104-m water column as documented by Ellis, Staal, and Chapman of DREA [7], [8]. The data utilized herein show resonance effects which are associated with acoustic interaction with a chalk bottom. The modeled sound-speed profile is shown in Fig. 18 with source and receiver depths of 38 and 71 m indicated by *S* and *R*, respectively. The sound-speed and depth values are listed in Table VI. Since the model is configured for a thin layer overlying the basement, the modeled bottom parameters, which are provided in Table VII, include a 2-m sediment layer overlying the chalk, which was not modeled by Ellis and Chapman.

A comparison of model results and the DREA model prediction to measured propagation loss from a source at 55-km range is shown in Fig. 19. The significant drop in propagation

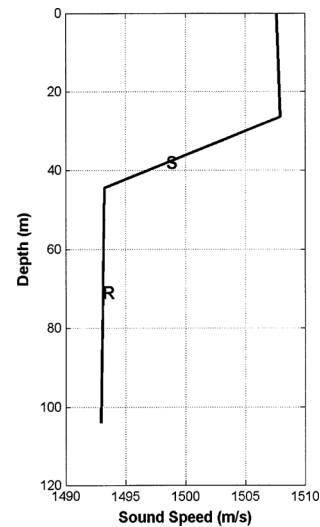


Fig. 18. Modeled sound-speed profile for data set 3; *S* and *R* denote source and receiver, respectively.

TABLE IV  
MODELED BOTTOM PARAMETERS FOR DATA SET 1; *f* IS FREQUENCY IN HERTZ

Parameter	Units	Value
Layer thickness	m	5
Sediment compressional sound speed	m/s	1780
Basement compressional sound speed	m/s	5500
Sediment shear sound speed	m/s	170
Basement shear sound speed	m/s	2400
Sediment compressional attenuation	dB/km	$0.7f$
Basement compressional attenuation	dB/km	$0.1f$
Sediment shear attenuation	dB/km	$13f$
Basement shear attenuation	dB/km	$0.06f$
Sediment density	$g/cm^3$	2
Basement density	$g/cm^3$	2.6

TABLE V  
MODELED BOTTOM PARAMETERS FOR DATA SET 2; *f* IS FREQUENCY IN HERTZ

Parameter	Units	Value
Layer thickness	m	6
Sediment compressional sound speed	m/s	1680
Basement compressional sound speed	m/s	5500
Sediment shear sound speed	m/s	200
Basement shear sound speed	m/s	3000
Sediment compressional attenuation	dB/km	$0.7f$
Basement compressional attenuation	dB/km	$0.1f$
Sediment shear attenuation	dB/km	$13f$
Basement shear attenuation	dB/km	$0.06f$
Sediment density	$g/cm^3$	2
Basement density	$g/cm^3$	2.6

at frequencies below about 300 Hz is again reproduced by the model(s).

### D. Data Set 4

The fourth data set is taken from efforts to model data gathered on the Eastern Canadian Continental Shelf over a hard rock (granite) seabed in a 150-m water column, as documented by Ellis, Chapman, Staal, and Hughes of DREA [9]–[12]. High losses between 10 and 100 Hz observed at a range of 13 km are believed to be the result of shear resonance effects. The modeled (near-iso) sound-speed profile is shown in Fig. 20 with source and receiver depths of 18.3 and 71 m indicated by *S* and *R*, respectively. The sound-speed and depth values are listed in

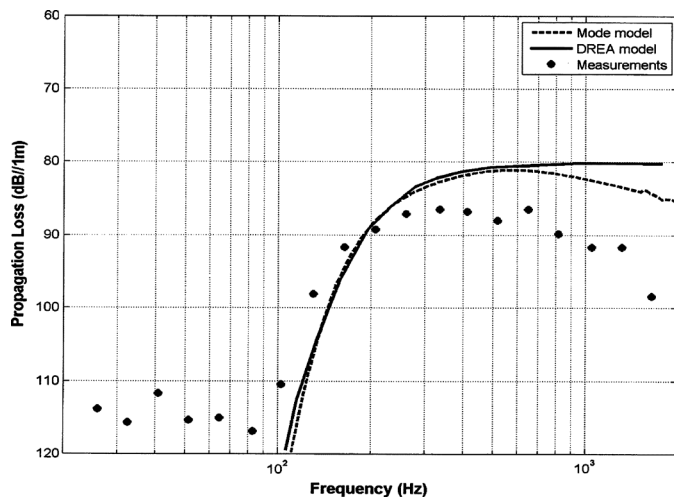


Fig. 19. Model comparison to measured propagation and DREA results to 55 km on the Continental Shelf of the British Isles (data set 3).

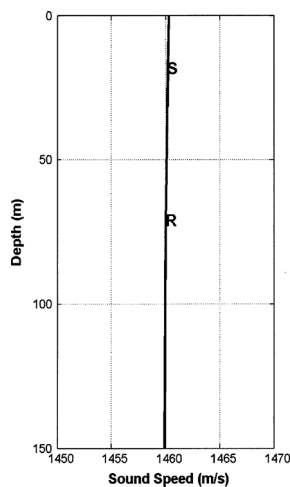


Fig. 20. Modeled sound-speed profile for data set 4;  $S$  and  $R$  denote source and receiver, respectively.

TABLE VI  
MODELED SOUND-SPEED PROFILE FOR DATA SET 3

Depth (m)	Sound speed (m/s)
0	1507.62
26.41	1507.91
44.39	1493.21
104	1492.93

Table VIII and the modeled bottom parameters are provided in Table IX.

A plot of the total reflection loss magnitude as a function of grazing angle and frequency is shown in Fig. 21. Comparison of Fig. 21 to [12, Fig. 10(a)] indicates the agreement with the calculations documented therein. Comparison of model results to propagation loss from a source at 13-km range, in addition to corresponding calculations made using the DREA [12] and Seismo-Acoustic Fast field Algorithm for Range-Independent environments (SAFARI) [26] models, are shown in Fig. 22. Although agreement with the measurements is generally poor, the significant resonance at about 25 Hz is reproduced by all of the models.

TABLE VII  
MODELED BOTTOM PARAMETERS FOR DATA SET 3;  $f$  IS FREQUENCY IN HERTZ

Parameter	Units	Value
Layer thickness	m	2
Sediment compressional sound speed	m/s	1700
Basement compressional sound speed	m/s	2400
Sediment shear sound speed	m/s	1000
Basement shear sound speed	m/s	1000
Sediment compressional attenuation	dB/km	$0.5f$
Basement compressional attenuation	dB/km	$0.1f$
Sediment shear attenuation	dB/km	$0.001f$
Basement shear attenuation	dB/km	$0.001f$
Sediment density	$g/cm^3$	1.9
Basement density	$g/cm^3$	2.2

TABLE VIII  
MODELED SOUND-SPEED PROFILE FOR DATA SET 4

Depth (m)	Sound speed (m/s)
0	1460.4
18.3	1460.3
45	1460.2
72	1460.1
150	1460

TABLE IX  
MODELED BOTTOM PARAMETERS FOR DATA SET 4;  $f$  IS FREQUENCY IN HERTZ

Parameter	Units	Value
Layer thickness	m	1.75
Sediment compressional sound speed	m/s	1780
Basement compressional sound speed	m/s	5500
Sediment shear sound speed	m/s	170
Basement shear sound speed	m/s	2400
Sediment compressional attenuation	dB/km	$0.7f$
Basement compressional attenuation	dB/km	$0.1f$
Sediment shear attenuation	dB/km	$13f$
Basement shear attenuation	dB/km	$0.06f$
Sediment density	$g/cm^3$	2.2
Basement density	$g/cm^3$	2.6

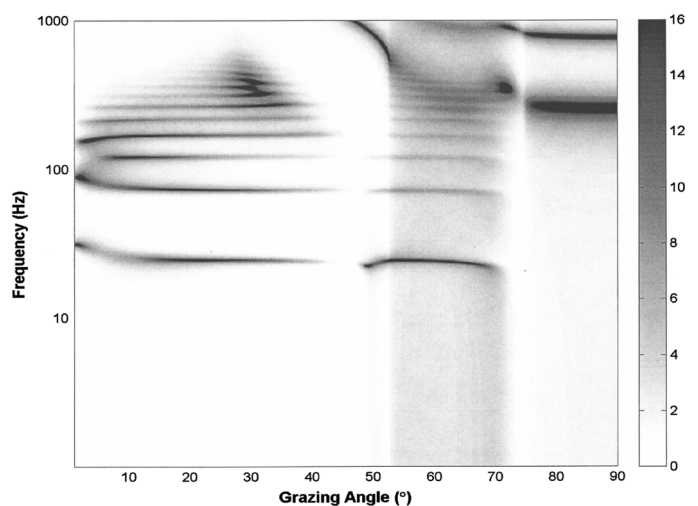


Fig. 21. Total bottom reflection loss in decibels for the Continental Shelf Environment of [12] (data set 4) (compare to [12, Fig. 10(a)]).

## VIII. SUMMARY

A bottom sediment model which incorporates compressional and shear reflection and transmission through a layered sediment into a single reflection coefficient for use in conjunction

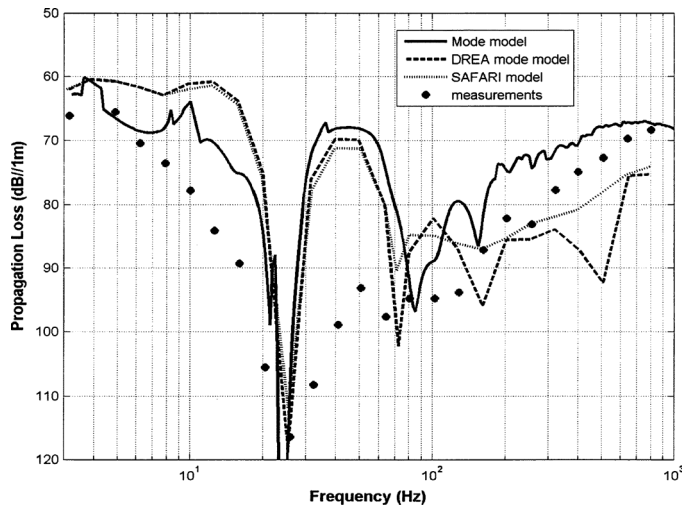


Fig. 22. Model comparison to measured propagation, SAFARI, and DREA predictions to 13 km in the Continental Shelf Environment of [12] (data set 4) (compare to [12, Fig. 7]).

with the normal mode model described in [24] has been presented. Calculation of individual transmission and reflection coefficients as a function of grazing angle has been benchmarked against known results [21]. The consolidation of bottom effects into a single reflection coefficient has been shown to enable successful reproduction of losses associated with bottom shear effects in a number of environments. The ability of the model to reproduce the measured data sets studied is comparable to that of the other models represented [3], [8], [26]. In addition, the approach enables isolation of the acoustic effects resulting from the interaction of various path types with the bottom sediment.

#### APPENDIX

To show that the infinite series in (30) converges, consider the elements of  $X$  as represented in (27). If we assume that  $|R_{pp0}| + |R_{ps0}|$ , and likewise the sums of the magnitudes of the coefficients in the rows of the two arrays comprising  $X$  are less than unity, then it is easy to show that the same is true of the matrix  $X$ , i.e., the sums of the magnitudes of the elements in each row are less than unity. Thus, if we multiply  $X$  times an arbitrary vector  $(x, y)^T$  and, without loss of generality, assume  $|y| \geq |x|$ , we have

$$\begin{pmatrix} x_{11} & x_{12} \\ x_{21} & x_{22} \end{pmatrix} \begin{pmatrix} x \\ y \end{pmatrix} = \begin{pmatrix} x_{11}x + x_{12}y \\ x_{21}x + x_{22}y \end{pmatrix}$$

and

$$\begin{aligned} |x_{11}x + x_{12}y| &< |x_{11}x| + |x_{12}y| = |x_{11}||x| + |x_{12}||y| \\ &\leq |x_{11}||y| + |x_{12}||y| = (|x_{11}| + |x_{12}|)|y| \leq |y|. \end{aligned}$$

Similarly,  $|x_{21}x + x_{22}y| \leq |y|$ , and since  $\lambda_{1,2}$  are eigenvalues for  $i = 1, 2$ , we have, for either eigenvalue  $\lambda$ ,  $|\lambda y| = |x_{21}x + x_{22}y| < |y|$ , which implies  $|\lambda| < 1$ , sufficing to ensure convergence.

#### ACKNOWLEDGMENT

The author would like to acknowledge Dr. G. A. Leibiger, formerly of the Naval Undersea Warfare Center (NUWC), in

partnership with whom the approach documented herein was originally developed.

#### REFERENCES

- [1] P. J. Vidmar, "The effect of sediment rigidity on bottom reflection loss in a typical deep sea sediment," *J. Acoust. Soc. Amer.*, vol. 68, no. 2, pp. 634–638, Aug. 1980.
- [2] P. J. Vidmar, "Ray path analysis of sediment shear wave effects on bottom reflection loss," *J. Acoust. Soc. Amer.*, vol. 68, no. 2, pp. 639–648, Aug. 1980.
- [3] J. H. Beebe and C. W. Holland, "The effect of unconsolidated sediment rigidity on low frequency acoustic propagation," in *Ocean Seismo-Acoustics, Low-Frequency Underwater Acoustics*, T. Akal and J. Berkson, Eds. New York: Plenum, 1986, pp. 207–215.
- [4] J. H. Beebe and S. T. McDaniel, "Geoacoustic models of the seabed to support range-dependent propagation studies on the Scotian Shelf," in *Bottom Interacting Ocean Acoustics*, W. A. Kuperman and F. B. Jensen, Eds. New York: Plenum, 1980, pp. 507–523.
- [5] S. T. McDaniel and J. H. Beebe, "Influence of semiconsolidated sediments on sound propagation in a coastal region," in *Bottom Interacting Ocean Acoustics*, W. A. Kuperman and F. B. Jensen, Eds. New York: Plenum, 1980, pp. 493–505.
- [6] J. H. Beebe and C. W. Holland, "Shallow-water propagation effects over a complex, high-velocity bottom," *J. Acoust. Soc. Amer.*, vol. 80, no. 1, pp. 244–250, Jul. 1986.
- [7] P. R. Staal, "Acoustic propagation measurements with a bottom mounted array," in *Acoustics and the Sea-Bed*, N. G. Pace, Ed. Bath, U.K.: Bath Univ. Press, 1983, pp. 289–296.
- [8] D. D. Ellis and D. M. F. Chapman, "Modelling of shear-wave related acoustic propagation on the UK continental shelf," Defence Research Establishment Atlantic (DREA), Halifax, NS, Canada, Tech. Memo. 84/P, Aug. 1984.
- [9] D. M. F. Chapman and D. D. Ellis, "Propagation modelling on the Scotian Shelf: The geoacoustic model," in *Bottom Interacting Ocean Acoustics*, W. A. Kuperman and F. B. Jensen, Eds. New York: Plenum, 1980, pp. 525–539.
- [10] D. D. Ellis and D. M. F. Chapman, "Propagation loss modelling on the Scotian Shelf: Comparison of model predictions with measurements," in *Bottom Interacting Ocean Acoustics*, W. A. Kuperman and F. B. Jensen, Eds. New York: Plenum, 1980, pp. 541–555.
- [11] P. R. Staal and D. M. F. Chapman, "Observations of interface waves and low-frequency acoustic propagation over a rough granite seabed," in *Ocean Seismo-Acoustics, Low-Frequency Underwater Acoustics*, T. Akal and J. Berkson, Eds. New York: Plenum, 1986, pp. 643–652.
- [12] S. J. Hughes, D. D. Ellis, D. M. F. Chapman, and P. R. Staal, "Low-frequency acoustic propagation loss in shallow water over hard-rock seabeds covered by a thin layer of elastic-solid sediment," *J. Acoust. Soc. Amer.*, vol. 88, no. 1, pp. 283–297, Jul. 1990.
- [13] M. Deschamps and C. Cao, "Reflection/refraction of a solid layer by Debye's series expansion," *Ultrasonics*, vol. 29, pp. 288–293, 1991.
- [14] S. I. Rokhlin and W. Huang, "Ultrasonic wave interaction with a thin anisotropic layer between two anisotropic solids; exact and asymptotic-boundary-condition methods," *J. Acoust. Soc. Amer.*, vol. 92, no. 3, pp. 1729–1742, Sep. 1992.
- [15] J. M. Hovem and A. Kristensen, "Reflection loss at a bottom with a fluid sediment layer over a hard solid half-space," *J. Acoust. Soc. Amer.*, vol. 92, no. 1, pp. 335–340, Jul. 1992.
- [16] N. R. Chapman and D. M. F. Chapman, "A coherent ray model of plane-wave reflection from a thin sediment layer," *J. Acoust. Soc. Amer.*, vol. 94, no. 5, pp. 2731–2738, Nov. 1993.
- [17] M. A. Ainslie, "Plane-wave reflection and transmission coefficients for a three-layered elastic bottom," *J. Acoust. Soc. Amer.*, vol. 97, no. 2, pp. 954–961, Feb. 1995.
- [18] M. A. Ainslie and P. W. Burns, "Energy-conserving reflection and transmission coefficients for a solid-solid boundary," *J. Acoust. Soc. Amer.*, vol. 98, no. 5, pp. 2836–2840, Nov. 1995.
- [19] D. Tollefsen, "Thin-sediment shear-induced effects on low-frequency broadband acoustic propagation in a shallow continental sea," *J. Acoust. Soc. Amer.*, vol. 104, no. 5, pp. 2718–2726, Nov. 1998.
- [20] M. A. Ainslie, "Conditions for the excitation of interface waves in a thin unconsolidated sediment layer," *J. Sound Vib.*, vol. 268, no. 2, pp. 249–267, 2003.
- [21] W. M. Ewing, W. S. Jardetzky, and F. Press, *Elastic Waves in Layered Media*. New York: McGraw-Hill, 1957.

- [22] K. Ergin, "Energy ratio of the seismic waves reflected and refracted at a rock-water boundary," *Bull. Seismol. Soc. Amer.*, vol. 42, pp. 349–372, 1952.
- [23] B. Gutenberg, "Erdbebenwellen V und VI," *Nachr. Akad. Wiss. Göttingen*, pp. 121–206 and 625–675, 1912.
- [24] C. A. Clark and K. B. Smith, "An efficient normal mode solution to wave propagation prediction," *IEEE J. Ocean. Eng.*, vol. 33, no. 4, pp. 462–476, Oct. 2008.
- [25] H. Schmidt and F. B. Jensen, "A full wave solution for propagation in multilayered viscoelastic media with application to Gaussian beam reflection at fluid-solid interfaces," *J. Acoust. Soc. Amer.*, vol. 77, no. 3, pp. 813–825, Mar. 1985.
- [26] H. Schmidt, "SAFARI: Seismo-Acoustic Fast field Algorithm for Range-Independent environments," La Spezia, Italy, SACLANTCEN Rep. SR-113, Sep. 1988.
- [27] L. M. Brekhovskikh, *Waves in Layered Media*, 2nd ed. New York: Academic, 1980.
- [28] D. F. McCammon and S. Hollingsworth, "Propagation in shallow water over high shear loss sediments; data vs fullmode," Pennsylvania State University, Appl. Res. Lab., Reston, VA, TM 90-281, Oct. 26, 1990.



**Cathy Ann Clark** (S'03–M'04–SM'12) received the B.S. degree in mathematics from Morehead State University, Morehead, KY, in 1970, the M.S. degree in mathematics from the University of Connecticut, Storrs, in 1976, and the M.S. degree in electrical engineering and the Ph.D. degree in applied mathematics from the University of Rhode Island, Kingston, in 2001 and 2004, respectively.

She was a Communications Systems Analyst with Western Union Corporation, Mahwah, NJ, from 1969 to 1973. From 1973 to 1979, she taught mathematics at the University of Connecticut and Connecticut community colleges. From 1979 to 1997, she was a Principal Analyst with Sonalysts, Inc., Waterford, CT, working with the Naval Undersea Warfare Center on underwater sound propagation modeling and submarine tactical decision aid development, and with the National Aeronautics and Space Administration on satellite communications. Since 1997, she has been with the Sensors & Sonar Systems Department, Naval Undersea Warfare Center, Newport, RI. Her research interests include underwater acoustics, boundary value problems, and difference equations.

Dr. Clark is a Senior Member of the IEEE Oceanic Engineering Society and a Fellow of the Acoustical Society of America.